

Fast Magnetic Twister and Plasma Perturbations in a 3-D Coronal Arcade

K. Murawski

Group of Astrophysics, UMCS, ul. Radziszewskiego 10, 20-031 Lublin, Poland

`kmur@kft.umcs.lublin.pl`

A. K. Srivastava

Department of Physics, Indian Institute of Technology (BHU), Varanasi-221005, India

`asrivastava.app@iitbhu.ac.in`

Z. E. Musielak

Department of Physics, University of Texas at Arlington, Arlington, TX 76019, USA

`zmusielak@uta.edu`

Received _____; accepted _____

The Astrophysical Journal

ABSTRACT

We present results of 3-D numerical simulations of a fast magnetic twister excited above a foot-point of the potential solar coronal arcade that is embedded in the solar atmosphere with the initial VAL-IIIC temperature profile, which is smoothly extended into the solar corona. With the use of the FLASH code, we solve 3-D ideal magnetohydrodynamic equations by specifying a twist in the azimuthal component of magnetic field in the solar chromosphere. The imposed perturbation generates torsional Alfvén waves as well as plasma swirls that reach the other foot-point of the arcade and partially reflect back from the transition region. The two vortex channels are evident in the generated twisted flux-tube with a fragmentation near its apex that results from the initial twist as well as from the morphology of the tube. The numerical results are compared to observational data of plasma motions in a solar prominence. The comparison shows that the numerical results and the data qualitatively agree even though the observed plasma motions occur over comparatively large spatio-temporal scales in the prominence.

Subject headings: magnetohydrodynamics (MHD): sun — arcade: sun—jet

1. Introduction

Vortex and swirling plasma motions are ubiquitous in the solar atmosphere. At small spatio-temporal scales the chromospheric swirling motions were discovered as super-tornadoes providing an alternative mechanism for channeling energy up to the inner solar corona (Wedemeyer-Böhm et al. 2012, 2013). Just after this novel observation, Su et al. (2013) reported the large-scale but slowly rotating coronal tornadoes. They studied the rotating vertical magnetic structures most likely driven by the underlying vortex flows in the photosphere that existed in a group with prominences. In case of such large-scale and slowly rotating tornadoes, which are long living magnetic structures, several other observational findings were made using recent space-borne observations (e.g., Panesar et al. 2013; Yan et al. 2013; Wedemeyer-Böhm et al. 2013; and references therein). However, recently the findings of Panasenco et al. (2014) poses a challenge to the large-scale coronal tornado detections. In the observational data they analyzed and found that the coronal tornado-like appearance usually associated with the prominences is mainly an illusion due to projection effects.

The fact that the projection effects can significantly distort the interpretation of such observations of coronal tornadoes is known. Similar effects could become important in interpretation of the solar observations of various localized plasma motions, such as plasma cyclones, swirls and tornadoes, which are ubiquitous in the solar corona, and whose origin, nature, morphology, life-time and driving mechanisms are difficult to observationally determine. Our numerical studies of magnetic twisters in solar coronal arcades presented in this paper are designed to address some of these currently unsolved problems.

The exact physical mechanisms responsible for the origin of long-lived coronal tornadoes are not fully known. Moreover, the relationship between the short-lived chromospheric tornadoes and the long-lived coronal tornadoes is also not well established. Shukla (2013)

developed a generalized theory, which implies that the modified-kinetic Alfvén waves (m-KAWs) in a magnetized plasma can propagate in the form of tornadoes, characterized by the plasma whirls or magnetic flux ropes carrying orbital angular momentum. Now, in the lower solar atmosphere, the small-scale chromospheric tornadoes may be caused by the photospheric vortices (e.g., Bonet et al. 2008; Shelyag et al. 2011; Murawski et al. 2013a,b, and references therein). Moreover, various types of these vortex motions could be associated with the different eddies and waves depending on the localized plasma and magnetic conditions as well as on the nature of the drivers/perturbations (Fedun et al. 2011; Murawski et al. 2013b). Therefore, it is important to understand the nature and generation of such swirling plasma motions in the different layers of the solar atmosphere, where various topologies of solar magnetic fields occur.

As far as the large-scale solar tornadoes are concerned, they are mostly observed in the association with the prominence legs (Su et al. 2012; Wedemeyer-Böhm et al. 2013), and are most likely related to the response of the photospheric vortices activated near the foot-points. These vortex flows exhibit spiral motions both upwards and downwards with speeds comparable to the values found for such tornado rotations in the form of prominence barbs (Wedemeyer-Böhm et al. 2012, Su et al. 2012). However, they are long-lived (on the time-scale of 12 – 24 hours) but slow rotators. There is another kind of interesting twisting and then swirl of the plasma around the core prominence magnetic field that may have the same origin due to rotation near the prominences' foot-point but entirely different when compared to the long-lived slow tornadoes. We call it a fast magnetic twister and associate it with a coronal arcade. This paper is devoted to numerical studies of such a phenomenon.

It must be pointed out that the fast magnetic twistings, which live on the time-scale of minutes, are seldomly observed in the solar atmosphere. Recently, Joshi et al. (2014) investigated a fast twisting prominence system in the context of its stability and reformation

that is significant for space-weather prediction. However, their aim was certainly not to understand the possible driver responsible for the evolution of fast magnetic twister and plasma swirl in the filament system that was initially bipolar in nature. It should also be noted that Shelyag et al. (2013) studied solar photospheric vortices by using MHD simulations with non-gray radiative transport and a non-ideal equation of state. The main difference between these two studies is that only the former takes into account variation of the local velocity field on time. As a result, the photospheric vortices (tornado-like motions) do not exist but instead torsional Alfvén waves are generated. We discuss this finding after we present the results of our numerical simulations.

In the present paper, we perform 3-D numerical simulations of the evolution of right-handed clock-wise twist and its responses in form of the torsional Alfvén and plasma perturbations in an initial potential field configuration of a magnetic flux-tube mimicking the observed prominence system. We call the magneto-plasma motions that evolved in our model "fast magnetic twistlers". Since 3-D numerical simulations in realistic atmosphere would be extremely computationally expensive to model the observed prominence flux-tube and its associated dynamics, we rescale the realistic very large spatio-temporal scales characteristic for the observational domain to a much smaller 3-D numerical simulation domain. Nevertheless, our simulation results match qualitatively the observed magnetic field and plasma dynamics as it is shown in our comparison between the numerical results and some recent solar observations.

This paper is organized as follows. In Sec. 2, we present the numerical simulation model. We outline the results of numerical simulations in the context of its physical significance in Sec. 3. In Sec. 4, we compare the numerical results with the relevant solar observational data. In the last section, we present discussion and concluding remarks.

2. Numerical Model and Results of Numerical Simulations

2.1. Governing Equations

We consider the following set of ideal MHD equations

$$\frac{\partial \varrho}{\partial t} + \nabla \cdot (\varrho \mathbf{V}) = 0, \quad (1)$$

$$\varrho \frac{\partial \mathbf{V}}{\partial t} + \varrho (\mathbf{V} \cdot \nabla) \mathbf{V} = -\nabla p + \frac{1}{\mu} (\nabla \times \mathbf{B}) \times \mathbf{B} + \varrho \mathbf{g}, \quad (2)$$

$$\frac{\partial p}{\partial t} + \nabla \cdot (p \mathbf{V}) = (1 - \gamma) p \nabla \cdot \mathbf{V}, \quad (3)$$

$$\frac{\partial \mathbf{B}}{\partial t} = \nabla \times (\mathbf{V} \times \mathbf{B}), \quad \nabla \cdot \mathbf{B} = 0, \quad (4)$$

where ϱ denotes mass density, $\mathbf{V} = [V_x, V_y, V_z]$ is the flow velocity, $\mathbf{B} = [B_x, B_y, B_z]$ is the magnetic field, p is the gas pressure, T is the temperature, μ represents the magnetic permeability, $\gamma = 5/3$ is the adiabatic index, $\mathbf{g} = (0, -g, 0)$ is the gravitational acceleration with its magnitude $g = 274 \text{ m s}^{-2}$ being the solar value, m denotes mean particle mass that is specified by mean molecular weight value of 0.6, and k_B is the Boltzmann's constant.

2.2. Equilibrium Configuration

We assume that the above set of MHD equations describes the solar atmosphere, which is initially in static equilibrium ($\mathbf{V}_e = \mathbf{0}$) with the pressure gradient balanced by the gravity force

$$-\nabla p_e + \varrho_e \mathbf{g} = \mathbf{0}, \quad (5)$$

and with ϱ_e and p_e being the equilibrium mass density and gas pressure, respectively. Using the ideal gas law and the y -component of Eq. (5), we obtain

$$p_e(y) = p_0 \exp \left[- \int_{y_r}^y \frac{dy'}{\Lambda(y')} \right], \quad \varrho_e(y) = \frac{p_e(y)}{g \Lambda(y)}, \quad (6)$$

where

$$\Lambda(y) = k_{\text{B}}T_e(y)/(mg) \quad (7)$$

is the pressure scale-height, and p_0 denotes the gas pressure at $y = y_r$.

We assume that the equilibrium temperature profile $T_e(y)$ of the solar atmosphere is given by the VAL-C (Vernazza et al. 1981) atmospheric model, which is smoothly extended into the solar corona (Fig. 1, the top panel). Then with Eq. (6), we obtain the corresponding gas pressure and mass density profiles (not shown). In this model the temperature reaches 1 MK at coronal heights and saturates at this level. The atmosphere is structured so that the solar photosphere occupies the region $0 < y < 0.5$ Mm, the solar chromosphere is sandwiched between $y = 0.5$ Mm and the transition region that is located at $y \simeq 2.7$ Mm. The temperature minimum is acquired at $y \simeq 0.9$ Mm (Fig. 1, top).

As a result of Eq. (5) a magnetic field must be force-free and the required condition is

$$(\nabla \times \mathbf{B}_e) \times \mathbf{B}_e = \mathbf{0} , \quad (8)$$

such that it satisfies the current free condition

$$\nabla \times \mathbf{B}_e = \mathbf{0} , \quad (9)$$

and it is specified by the magnetic flux function, $A(x, y)$, defined by

$$\mathbf{B}_e = \nabla \times (A\hat{\mathbf{z}}) , \quad (10)$$

where the subscript $_e$ corresponds to equilibrium quantities and $\hat{\mathbf{z}}$ is a unit vector along z -direction.

We set an arcade magnetic field by choosing

$$A(x, y) = \frac{b}{2}B_0 \ln[x^2 + (y - b)^2] \quad (11)$$

with B_0 being the magnetic field at the reference level and b being the vertical coordinate of the singularity. We set and hold fixed $b = -5$ Mm while B_0 is determined from the following condition:

$$c_A(x = 0, y = y_r) = 10c_s(y = y_r), \quad (12)$$

where the Alfvén, c_A , and sound, c_s , speeds are given by

$$c_A(x, y) = \sqrt{\frac{B_e^2(x, y)}{\mu \rho_e(y)}}, \quad c_s(y) = \sqrt{\frac{\gamma p_e(y)}{\rho_e(y)}}, \quad (13)$$

and $y_r = 10$ Mm is the reference level that we choose in the solar corona at $y_r = 10$ Mm. The corresponding magnetic field-lines are displayed in Fig. 1 (the bottom panel).

2.3. Results of Numerical Simulation

We solved the set of MHD equations (1)-(4) numerically using the FLASH code (Lee and Deane 2009, Lee 2013). This code implements a second-order unsplit Godunov solver with various slope limiters and Riemann solvers. We set the simulation box as $(-15, 15)$ Mm \times $(1.75, 19.75)$ Mm \times $(-3, 3)$ Mm. At the top, bottom, left- and right-hand sides of the numerical domain we imposed the boundary conditions by fixing in time all plasma quantities to their equilibrium values, while along z we implemented open boundaries. Additionally, at the bottom boundary a twist in the azimuthal component of magnetic field, B_θ , was specified using

$$B_\theta(x, y, t) = -A_B r_h \exp \left[-\frac{r_h^2 + (y - y_0)^2}{w^2} \right] \left[\exp \left(\frac{t}{\tau} \right) - 1 \right], \quad (14)$$

where $r_h^2 \equiv (x - x_0)^2 + (z - z_0)^2$, A_B is the amplitude of the pulse, (x_0, y_0, z_0) is its position, w denotes its width, and τ is a growing time of the implemented twist. We set and hold fixed $A_B = 0.05$ Tesla, $x_0 = -10$ Mm, $y_0 = 1.75$ Mm, $z_0 = 0$ Mm, $w = 0.3$ Mm, and $\tau = 100$ s. Therefore, the spatial scale of numerical domain is 18 Mm in the vertical direction, 30 Mm

in the horizontal x -direction, and 6 Mm in the horizontal z -direction. In our simulations, we use an Adaptive Mesh Refinement (AMR) grid with a minimum (maximum) level of refinement set to 2 (5). The extent of the simulation box in the y -direction ensures that we catch the essential physics occurring in the solar photosphere-low corona domain, and minimize the effect of spurious signal reflections from the top boundary. As each block consists of $8 \times 8 \times 8$ identical numerical cells, we reach the effective finest spatial resolution of about 0.24 Mm, below the altitude $y = 3.25$ Mm. The initial system of blocks is shown in Figure 2.

Fig. 3 shows a development of the initial magnetic field configuration of an initially potential arcade embedded in the corona whose foot-points were anchored in the photosphere. The magnetic field lines were initially parallel to each other without any twist present. We applied a twist in the B_θ component of the magnetic field (Eq. 14) above the photosphere. The figure displays the activation of a right-handed clockwise twist in the magnetic field near the chromosphere into the corona. The snapshots respectively represent the following times: $t = 50$ s, $t = 75$ s, $t = 100$ s, $t = 125$ s shown from the top-left to bottom-right panels. Red, green, and blue arrows correspond to the x -, y -, and z -axis, respectively, and such notation is used in all 3-D figures throughout this paper. It is clear that initially the azimuthal component of magnetic field lines warps within the ambient potential field as per the right-handed twisting (top-left). However, at the later times, the twisting scenario becomes more complex and it does not remain in the state of ideal right-handed circular twist. Instead, the depression from one-side is seen in the chromospheric region that makes the evolution of eight-shape complex twisting of the magnetic field lines near the foot-point of the flux-tube. On the contrary, the right-handed twist evolves more ideally circularly at the coronal heights as shown in Fig. 3 (the top-right and bottom-left panels). The shearing of whole flux-tube is also evident during the activation of the twist and its propagation higher into the corona (see the bottom-right

panel in Fig. 3).

Fig. 4 illustrates evolution of the magnetic field lines in the zoomed region that is located close to the implemented twist in B_θ . The initially parallel magnetic field lines become changed after applying a twist in the B_θ component of the magnetic field (see Eq. 14). This figure displays the evolution of a right-handed clockwise twist in the magnetic field of the flux-rope from its chromospheric view point in the plane perpendicular to our line-of-sight (LOS). The snapshots respectively represent the following times: $t = 50$ s (the top-left panel), $t = 75$ s (the top-right panel), $t = 100$ s (the bottom-left panel), and $t = 125$ s (the bottom-right panel). It is clear that at $t = 50$ s the twist is applied at the left foot-point and the magnetic field lines start bending from left-to-right (clock-wise), which is the sign of right-handed positive twist (top-left). Then, this twist grows in the coronal heights along the equilibrium initial magnetic field configuration (the top-right, bottom-left, bottom-right panels).

Fig. 5 shows the temporal snapshots of streamlines in the velocity field. These streamlines are given by

$$\frac{dx}{V_x} = \frac{dy}{V_y} = \frac{dz}{V_z}. \quad (15)$$

The figure displays the activation of a plasma swirling motion. The snapshots respectively represent the following times: $t = 50$ s, $t = 75$ s, $t = 100$ s, and $t = 125$ s as shown from the top-left to bottom-right panels. The plasma starts swirling and also rising up in the twisted magnetic fields. At the time $t = 50$ s, the helical (right-handed) swirling motion is more evolved and it reached another foot-point at $t = 100$ s (the top-right panel). Indeed these are fast perturbations moving inside the flux-tube from left foot-point to the right foot-point with a speed of about 500 km s^{-1} . The perturbations are the torsional Alfvén wave-like fast perturbations triggered in the considered coronal arcade system. The plasma motion is very complex as it is seen in the evolution of two vortex channels in the

presented snapshots. Moreover, the whole arcade system whips in the vertical direction, which may be the effect of kink instability seeded by twisted magnetic field lines. Finally, after the full activation of the twist, the arcade system possess torsional Alfvén wave-like fast perturbations, two parallel vortex channels, and plasma swirling in them. We shall discuss their physical consequences in the next section.

Fig. 6 displays the mass density maps in X-Z plane at the following times: $t = 50$ s (the top-left panel), $t = 75$ s (the top-right panel), $t = 100$ s (the bottom-left panel), and $t = 125$ s (the bottom-right panel). The evolution of shock front along the magnetic field lines and the complex plasma motions are evident in these snapshots. Again, the plasma motion is very complex because it is associated with the two vortex systems and their plasma swirling. The twisted magnetic field lines squeeze the chromospheric plasma and push it upwards (the top-left panel). Some plasma becomes detached as shown in the top-right panel. However, the plasma finally spreads over the curved interfaces. This overall dynamical scenario is associated with the evolution of the fast magnetic twister and the plasma perturbations in the large-scale magnetic structure.

3. Physical Interpretation

The results of our numerical simulations clearly show the presence of shearing, complex evolution and fragmentation of the twist as well as the generation of two sets of vortex channels, and the excitation of the fast torsional Alfvén wave-like perturbations in both channels (Figs. 3-6). The possible underlying physical scenarios are discussed below.

It is seen that some shearing occurs in the whole body of the evolved twisted magnetic flux-tube up to the corona (cf., Fig. 4). The underlying physics reveals that the shearing motions are generated by the competing actions of the Lorentz force and the gravity. Thus,

these two forces are responsible for driving the two counter-rotating twisters. As the cross section of these twisters expands due to the stratification in the solar atmosphere, the mass density (or a gas pressure) stratification of the plasma causes the upper parts of the twister to expand while the lower part remains constricted in the solar chromosphere, which results in the shearing as evident in our numerical results. Such shearing of the loops were first reported by Manchester (2003) and Manchester et al. (2004).

Depending on the initial degree of twist, portions of the magnetic flux-tube shed vortex pairs, and the magnetic flux is redistributed in the tube cross section in such a way that much of the flux is located away from the tube’s central axis. This phenomenon is known as the fragmentation of the tube and it was already recognized in the emerging bipolar flux-tubes from the sub-photospheric layers in the outer solar atmosphere with some twists (e.g., Abbett et al. 2000, Srivastava et al. 2010). However, the first numerical evidence for the generation of such fragmentation is clearly given by the results of our 3-D simulations of the activation of twist in the coronal arcade. The rising bipolar magnetic flux-tubes from the solar convection zone up to the photosphere can undergo the fragmentation if their initial twist is less than a critical twist and the curvature of the apex is small (Abbett et al. 2000). Our numerical simulations do support this already established physical picture.

Another interesting phenomenon seen in our 3D numerical simulations is that the velocity streamlines over the two vortex pairs reach the other foot-point of the magnetic flux-tube with an average speed of about $400 - 500 \text{ km s}^{-1}$, which is associated with the fast moving (with the Alfvén speed) perturbation. This is the most likely evolution of torsional Alfvén perturbations generated during twisting of the magnetic field lines and associated with the swirl/vortex motions.

The recent work by Shelyag et al. (2013) shows that the solar photospheric vortices do not exist because the perturbations used by these authors produce torsional Alfvén waves

instead. This is an interesting result, which is related to vortices in the intergranular cells that occur on smaller spatial and temporal scales than those considered in this paper. In our case, the large-scale magnetic system does show both the vortex channels as well as torsional Alfvén waves.

4. Qualitative Match of the Numerical Results with the Observations

We now describe observational data obtained for a solar prominence and make comparison between the data and our numerical results. Since there is a significant difference in spatio-temporal scales between the observed prominence and the numerically simulated fast magnetic twister in an arcade, the comparison can only be qualitative. Nevertheless, a qualitative agreement between the data and theory can be seen.

On 4 August, 2013 during 11:20 -12:20 UT there was an interesting plasma motion seen near the disk-centre in the south-east quadrant of the Sun. An almost bipolar core filament was lying quiescently, and suddenly some twisting and brightening occurred at its left foot-point; the nature of this twist was right-handed and clockwise (see Fig. 7 and movie Twisted-Filament.mp4). The figure and movie clearly show plasma swirls from the left-to-right clockwise, and fine structured motions of the plasma reached at another foot-point of the filament flux-rope system in almost 1800 s with the average speed of $\sim 400 \text{ km s}^{-1}$. It should be noted that almost semi-circular flux-rope system has the length $\sim 700 \text{ Mm}$, while the width near its apex was almost 70 Mm (cf., 11:49 UT snapshot) in the projection. The average speed of the moving perturbations from the left to right foot-point is indeed a fast speed. The plasma motions show some fragmentation of the path (see the 11:49 UT snapshot) and they convert into a very complex interaction between the two fragmented branches; as a result of this interaction a shallow apex is created with an apparent dip (see the 11:59 UT snapshot). The opposite plasma motions are

also evident in the remaining time span up to some extent, while the main right-handed vortex or swirl motions still continue for the next 30 minutes (see the attached movie Twisted-Filament.mp4).

Since we view the plasma motions in a filament plane that is almost perpendicular to the LOS, we compare the results of our numerical simulations (see Fig. 3) to the observations (see Fig. 7 and the movie). As already mentioned above, the comparison can only be qualitative because of the differences in scales between the numerical results and the data; our simulation domain must be re-scaled by factor of 24 in the flux-tube length, by 10 in the width (or spread of perturbations) near the apex, and by 10 in the time-scale in order to match the data. The comparison shows that the numerical results qualitatively match the observed magnetic field and plasma dynamics of the filament. For example, let us compare the 11:29 UT image in Fig. 7 to the top-left snapshots of Figs. 3-4. Then, the activation of magnetic twists (black filament threads in Fig. 7 and twists in the magnetic field lines (magenta colors) in Fig. 3) can clearly be seen. An initiation of the bright plasma swirl/vortex motions (the bright right-handed turning of the plasma envelope as shown in Fig. 7 and vortex in the magnetic field lines (magenta colors) in Fig. 3) also match with each other.

At the later times, the magnetic twists as well as the vortex motion of the plasma are evident both in the numerical simulations as well as in the observations. The fragmentation can be seen near the apex of the prominence fine structured plasma motions, where the formation of the two vortex channels in the numerical domain (cf., Fig. 7, bottom-right and Fig. 5, bottom) takes place. Now, the process of formation of the fragmented two vortex channels becomes evident in our numerical simulations (shape of eight in Figs. 4 and 5) than in the observations. The reason is that the real twist in the observational regime may differ from that considered in our model. Moreover, as stated above, the

fragmentation of the vortex/swirls of the plasma along the two channels can also be seen in Fig. 7. It must be noted nothing that both the observed and simulated vortex channels are associated with fast speeds that are the signatures of the evolution of the torsional Alfvén wave perturbations moving through these channels in a large-scale prominence-like bipolar magnetic structure. We referred to the observed and simulated phenomena as the fast magnetic twisters associated with the torsional perturbations and fast vortex motions.

5. Discussion and Concluding Remarks

We investigated numerically physical implications of the activation of the magnetic twists in a potential coronal magnetic flux-tube embedded in the solar atmosphere with a realistic temperature distribution. Our numerical results reveal the evolution of right-handed magnetic twists, double vortex channels, fragmentation and fast propagating perturbations, all evident in our coronal arcade model in which variable twists in the azimuthal component of the magnetic field were initially imposed. The result is a fast magnetic twister whose existence is reported here for the first time.

The initial perturbations imposed in our coronal arcade model generate torsional Alfvén waves as well as plasma swirls that reach the other foot-point of the arcade and partially reflect back from the transition region. The two vortex channels are evident in the generated twisted flux-tube with a fragmentation near its apex that results from the initial twist as well as from the morphology of the tube. This highly depends upon the initial magnetic field configuration, plasma properties, and nature of perturbations, which all determine how the vortices, associated waves and plasma motions are formed.

There were some previous studies of vortex motions at various spatio-temporal scales (e.g., Bonet et al. 2008; Shelyag et al. 2011; however, in none of them the fast magnetic

twister was identified. Moreover, Shelyag et al. (2013) reported no vortices (tornado-like motions) in their numerical simulations but only torsional Alfvén waves. We do see both fast magnetic twisters and torsional Alfvén waves. The difference between their approach and ours is in temporal scales, which in their approach are much shorter than in ours. Based on our results, we conclude that a tornado needs a long lasting twist in order to be sustained for time scales of the order of 12 hours or longer.

Our numerical results were compared to the observational data of plasma motions in a solar prominence, whose rare observation showed the evidence for the existence of a fast twister. Interestingly enough, the general properties of this twister are similar to those seen in our numerical simulations. However, we could only show that our numerical results and the data agreed only qualitatively because significant differences in the spatio-temporal scales between the observations and our numerical simulations prevented us from making a more direct comparison. In the future, more observations are needed to establish validity of our coronal arcade model at various spatio-temporal scales, and to examine if the double vortex system, plasma swirling, and fast torsional perturbations, all exist in a single prominence system before its eruption.

6. Acknowledgments

The authors are indebted to an anonymous referee whose valuable comments and suggestions allowed us to significantly improve the paper. This work was supported by NSF under the grant AGS 1246074 (K.M. and Z.E.M.). A.K.S. acknowledges a support during his stay at UMCS in Lublin, Poland, when a significant portion of this work was done. He also thanks Dr. N.C. Joshi for providing the observational data and animation, as well as Shobhna for patient encouragements. Z.E.M. acknowledges the support of this work by the Alexander von Humboldt Foundation, and by University of Texas at Arlington through its Faculty Development Program. We also acknowledge the use of the SDO/AIA observations for this study, with the data provided courtesy of NASA/SDO, LMSAL, and the AIA, EVE, and HMI science teams. The FLASH code used in our numerical simulations was developed by the DOE-supported ASC/Alliance Center for Astrophysical Thermonuclear Flashes at the University of Chicago. A.K.S. (and other co-authors) dedicate this work to one of the pioneering plasma physicists Prof. P.K. Shukla (7 July, 1950–26 January, 2013), Ruhr-University Bochum (RUB), Germany, who also had a doctoral degree in Department of Applied Physics, I.T.BHU, Varanasi, India in 1972, where he also completed his doctoral research in 2006.

REFERENCES

- Abbett, W.P., Fisher, G.H., & Fan, Y. 2000, *ApJ*, 540, 548
- Bonet, J.A., Márquez, I., Sánchez Almeida, J., Cabello, I., & Domingo, V. 2008, *ApJ*, 687, L131
- Fedun, V., Shelyag, S., Verth, G., Erdélyi, R., 2011, *An. Geo.*, 29, 1029
- Joshi, N.C., Srivastava, A.K., Filippov, Boris, Kayshap, P., Uddin, Wahab, Chandra, Ramesh, Choudhary, D.P., Dwivedi, B.N. 2013, *ApJ*, in press (doi:10.1088/0004-637X/785/1/1)
- Lee, D., Deane, A.E. 2009, *CoPh*, 228, 952
- Lee, D. 2013, *JCoPh*, 243, 269
- Manchester, W., IV, Gombosi, T., DeZeeuw, D., & Fan, Y. 2004, *ApJ*, 610, 588
- Manchester, W. 2003, *J. Geophys. Res. (Space Phys.)*, 108, 1162
- Murawski, K., Srivastava, A.K., McLaughlin, J.A., & Oliver, R. 2013a, *Sol. Phys.*, 283, 383
- Murawski, K., Ballai, I., Srivastava, A.K., & Lee, D. 2013b, *MNRAS*, 436, 1268
- Panesar, N.K., Innes, D.E., Tiwari, S.K., & Low, B.C. 2013, *A&A*, 549, A105
- Panasenco, O., Martin, S.F., & Velli, M. 2014, *Sol. Phys.*, 289, 603
- Shelyag, S., Keys, P., Mathioudakis, M., & Keenan, F.P. 2011, *A&A*, 526, A5
- Shelyag, S., Cally, P.S., Reid, A., & Mathioudakis, M. 2013, *ApJ*, 776, L4
- Shukla, P.K. 2013, *J. Geophys. Res. (Space Phys.)*, 118, 1
- Srivastava, A.K., Zaqarashvili, T.V., Kumar, P., & Khodachenko, M.L. 2010, *ApJ*, 715, 292

Su, Y., Wang, T., Veronig, A., Temmer, M., & Gan, W. 2012, *ApJ*, 756, L41

Vernazza, J.E., Avrett, E.H., & Loeser, R. 1981, *ApJS*, 45, 635

Wedemeyer-Böhm, S., Scullion, E., Steiner, O., et al. 2012, *Nature*, 486, 505

Wedemeyer-Böhm, S., Scullion, E., Rouppe van der Voort, L., Bosnjak, A., & Antolin, P.
2013, *ApJ*, 774, 123

Yan, X.L., Pan, G.M., Liu, J.H., et al. 2013, *AJ*, 145, 153

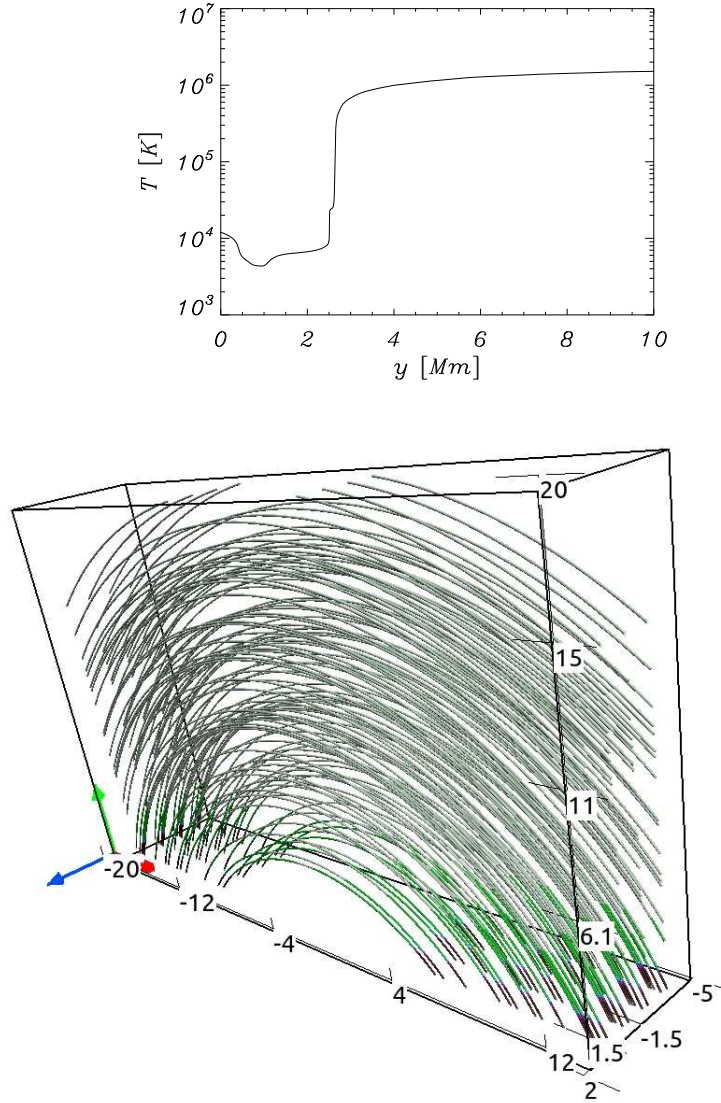


Fig. 1.— Equilibrium profiles of temperature (top panel) and magnetic field lines (bottom panel). The 3D visualization of the simulation data is carried out using the VAPOR (Visualization and Analysis Platform) software package.

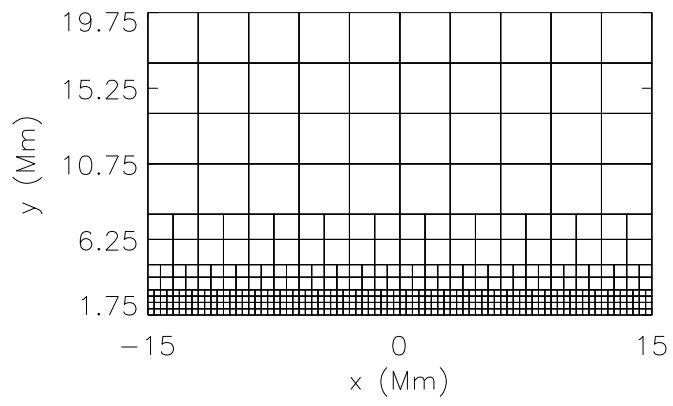


Fig. 2.— Numerical blocks with their boundaries (solid lines) at $t = 0$ s in the vertical plane ($z = 0$).

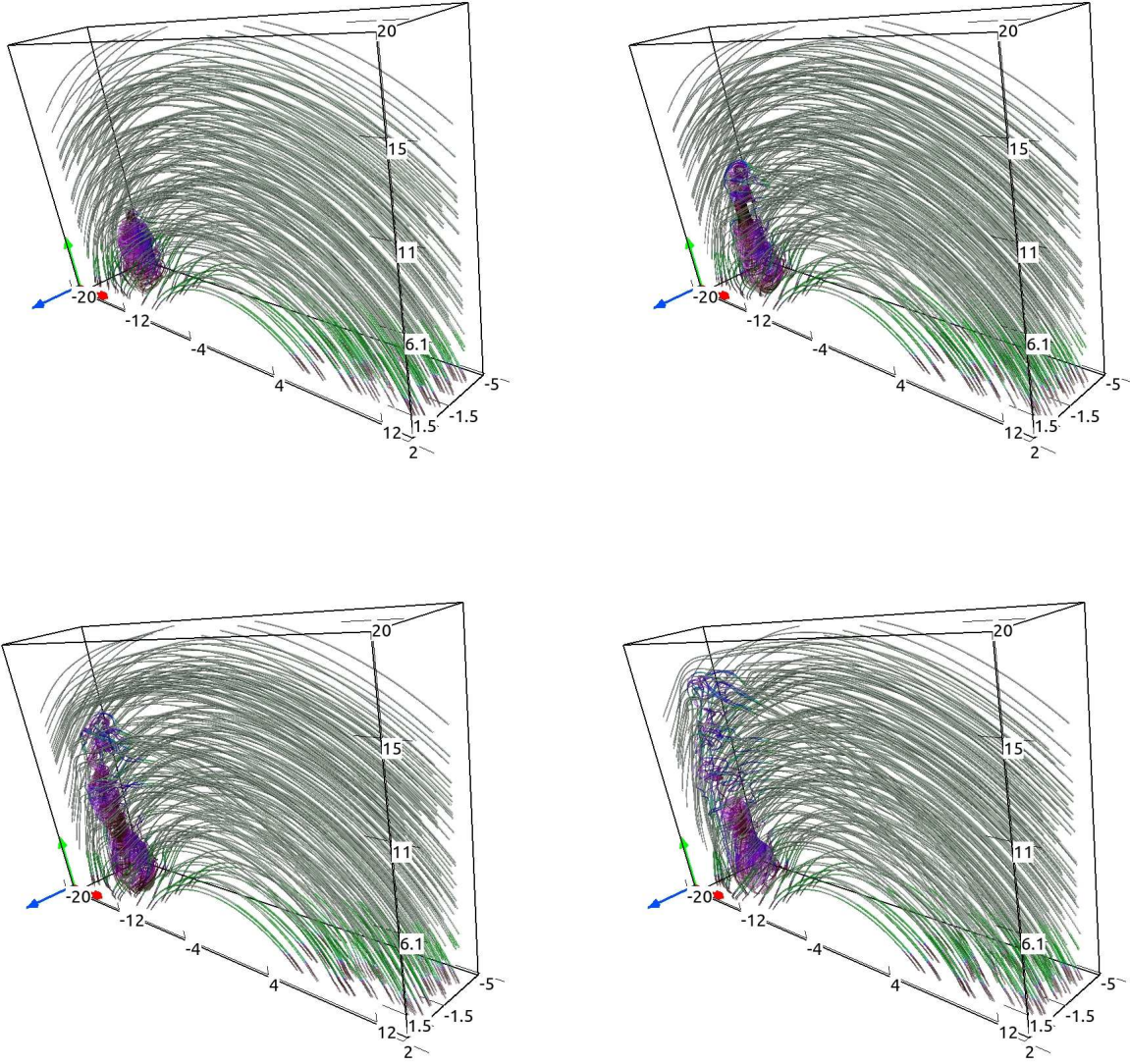


Fig. 3.— Activation of right-handed clockwise twist in the magnetic field of the flux-rope in corona at $t = 50$ s (top-left), $t = 75$ s (top-right), $t = 100$ s (bottom-left), $t = 125$ s (bottom-right). Red, green, and blue arrows correspond to the x -, y -, and z -axis, respectively.

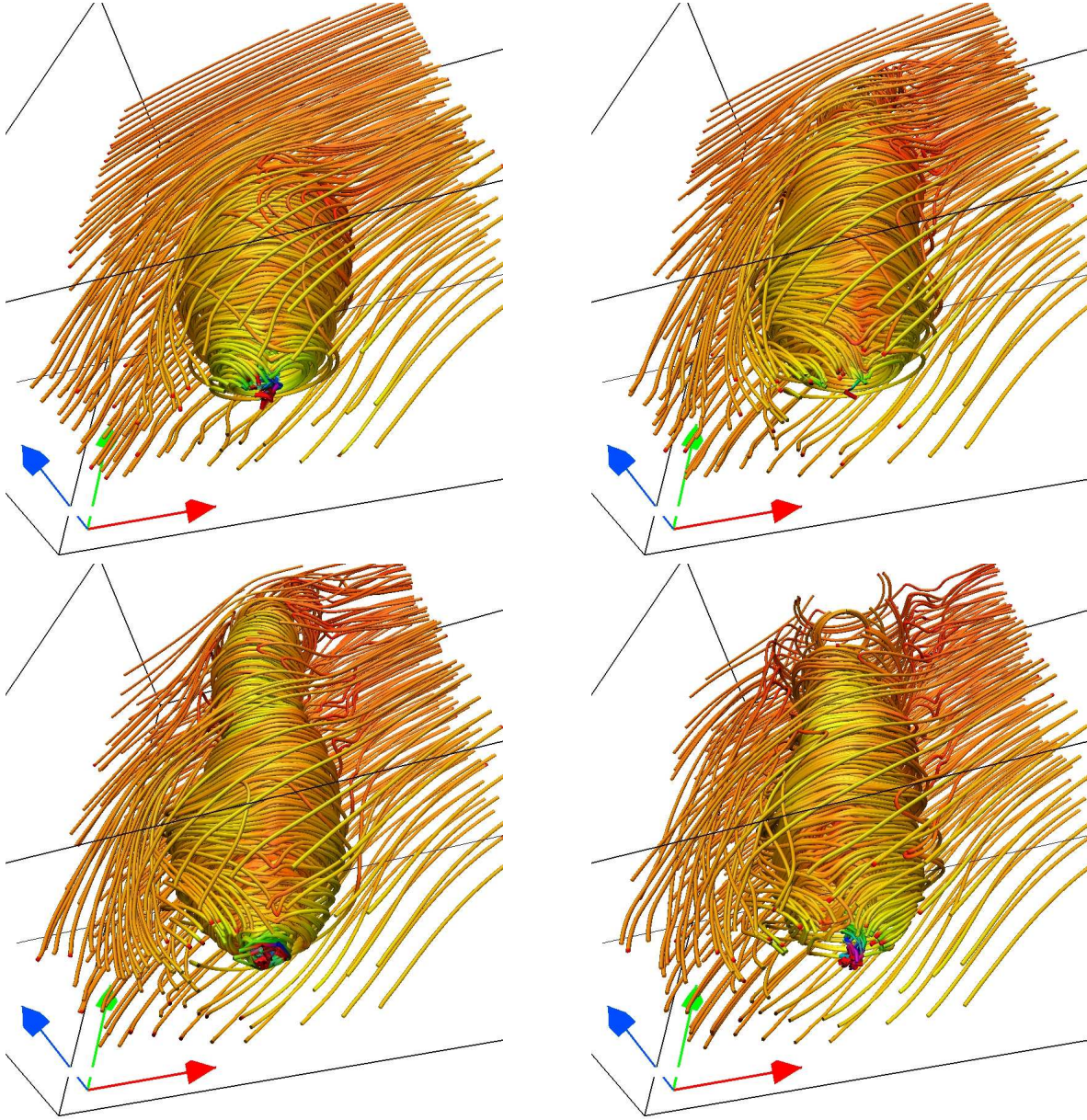


Fig. 4.— Activation of right-handed clockwise twist in the magnetic field of the flux-rope seen from near the photosphere at $t = 50$ s (top-left), $t = 75$ s (top-right), $t = 100$ s (bottom-left), $t = 125$ s (bottom-right).

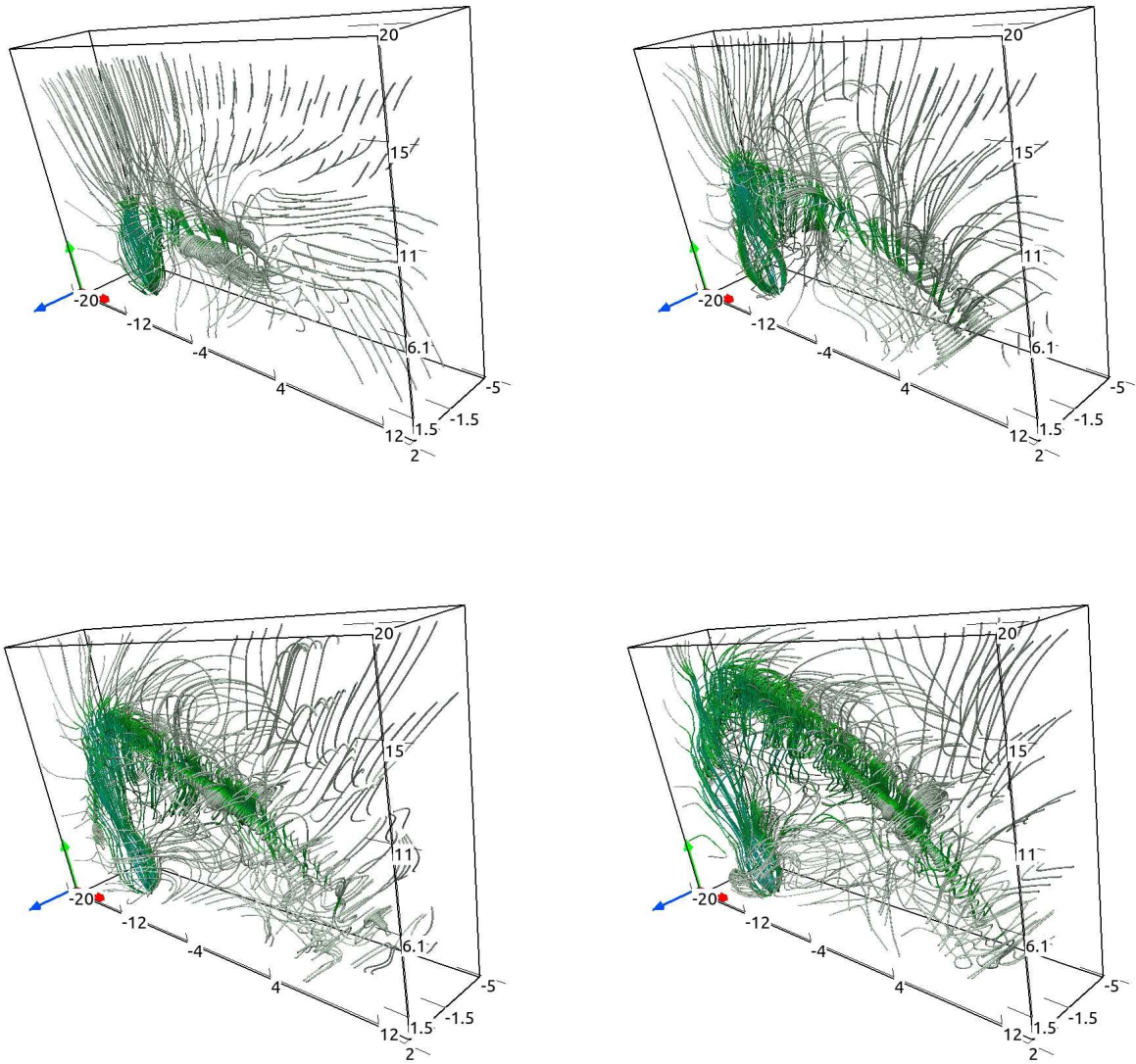


Fig. 5.— Streamlines at $t = 50$ s (top-left), $t = 75$ s (top-right), $t = 100$ s (bottom-left), and $t = 125$ s (bottom-right).

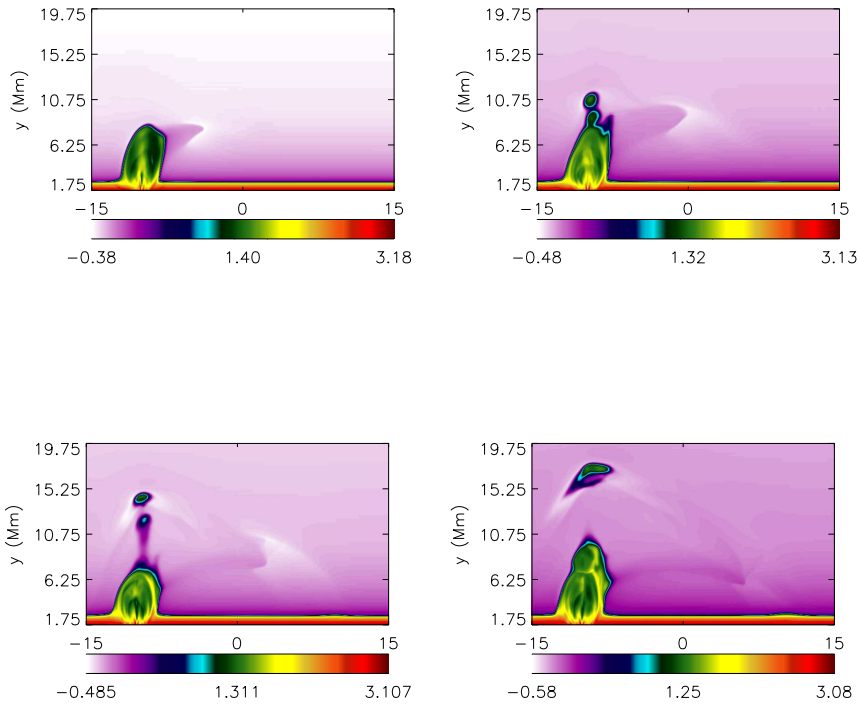


Fig. 6.— The mass density maps in X-Y plane (for $z = 0$) at times $t = 50$ s, $t = 75$ s, $t = 100$ s, and $t = 125$ s. The evolution of shock front along the flux-rope field lines and the complex plasma motions are evident.

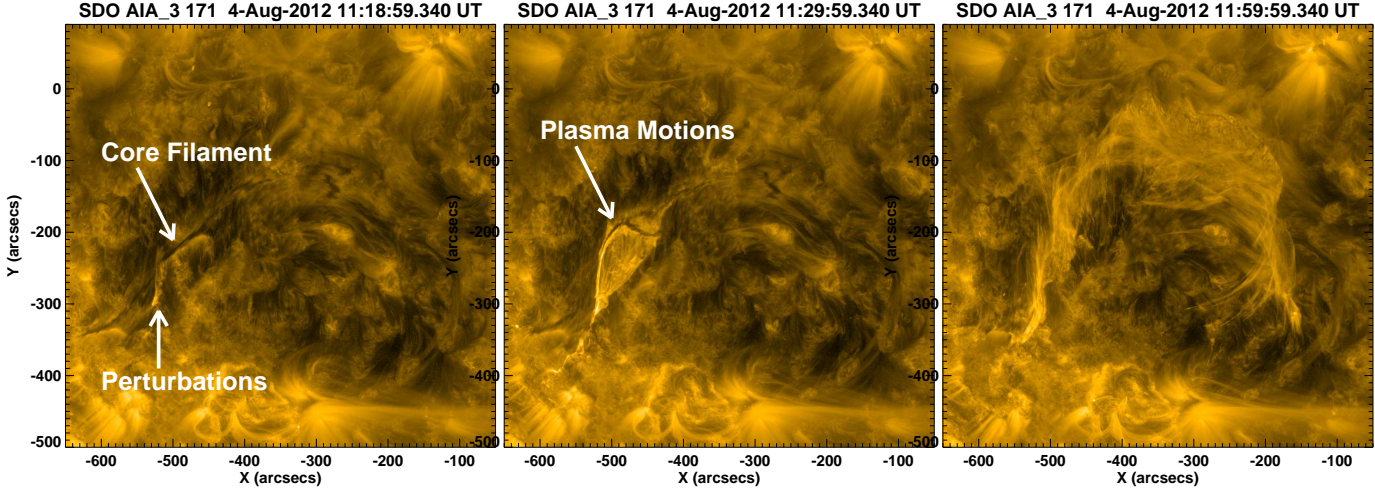
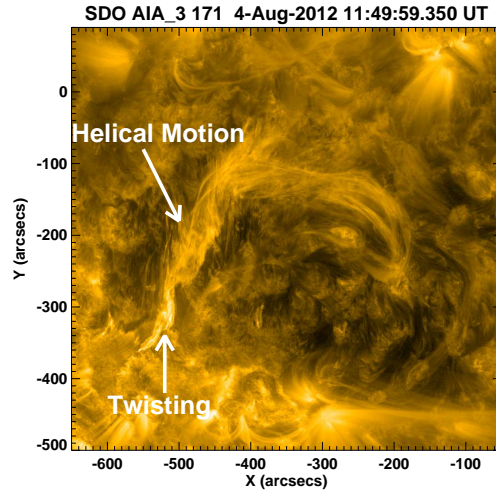


Fig. 7.— Qualitative description of an activation of similar helical twists and associated mass motion around a bipolar filament system though at large spatio-temporal scale adopted from Joshi et al. (2014).